First-in-human evaluation of cutaneous innate and adaptive immunomodulation by mosquito bites

David Guerrero[1,*], Hoa Thi My Vo[1,*], Chanthap Lon[3,*], Jennifer A. Bohl[2], Sreynik Nhik[3], Sophana Chea[3], Somnang Man[3,4], Sokunthea Sreng[3,4], Andrea R. Pacheco[3], Sokna Ly[3], Rathanak Sath[3], Sokchea Lay[1], Dorothee Missé[5], Rekol Huy[4], Rithea Leang[4], Hok Kry[6], Jesus G. Valenzuela[2], Fabiano Oliveira[2,$],Tineke Cantaert[1,$], Jessica E. Manning[2,3,$,#]

[1] Institut Pasteur du Cambodge, Pasteur Network, Phnom Penh, Cambodia

[2] Laboratory of Malaria and Vector Research, National Institute of Allergy and Infectious Diseases, National Institutes of Health, Rockville, Maryland, USA

[3] International Center of Excellence in Research, National Institute of Allergy and Infectious Diseases, National Institutes of Health, Phnom Penh, Cambodia

[4] National Center of Parasitology, Entomology, and Malaria Control, Phnom Penh, Cambodia

[5] MIVEGEC, Univ Montpellier, IRD, CNRS, 34000 Montpellier, France.

[6] Kampong Speu Provincial District, Ministry of Health, Phnom Penh, Cambodia

*co-first author

$ co-last author

corresponding author: jessica.manning@nih.gov

22   **Abstract**

23   Mosquito-borne viruses are a growing global threat. Initial viral inoculation occurs in the skin via

24   the mosquito 'bite', eliciting immune responses that shape the establishment of infection and

25   pathogenesis. We aimed to cutaneous innate and adaptive immune responses to mosquito bites in

26   individuals from endemic areas. In this single-arm, cross-sectional interventional study, we

27   enrolled 30 healthy adult participants aged 18 to 45 years of age from Cambodia between October

28   2020 and January 2021. We performed 3-mm skin biopsies at baseline as well as 30 minutes, 4

29   hours, and 48 hours after a controlled feeding by uninfected *Aedes aegypti* mosquitos. The primary

30   endpoints were measurement of changes in early and late innate responses in bitten vs unbitten

31   skin by gene expression profiling, immunophenotyping, and cytokine profiling. Results revealed

32   induction of neutrophil degranulation and recruitment of skin-resident dendritic cells and M2-

33   macrophages in 'bitten' skin. As the immune reaction progressed over time, T cell priming and

34   regulatory pathways were upregulated along with a shift to a Th2-driven response and CD8+ T

35   cell activation. In accordance, participants' bitten skin cells produced less pro-inflammatory

36   cytokines when stimulated by *Ae. aegypti* salivary gland extract. No unexpected adverse events

37   occurred, and one patient was lost to follow-up at Day 14. These results identify key immune

38   genes, cell types, and pathways in the human response to mosquito bites that can be leveraged to

39   develop novel therapeutics and vector-targeted vaccine candidates to arboviral diseases.

40
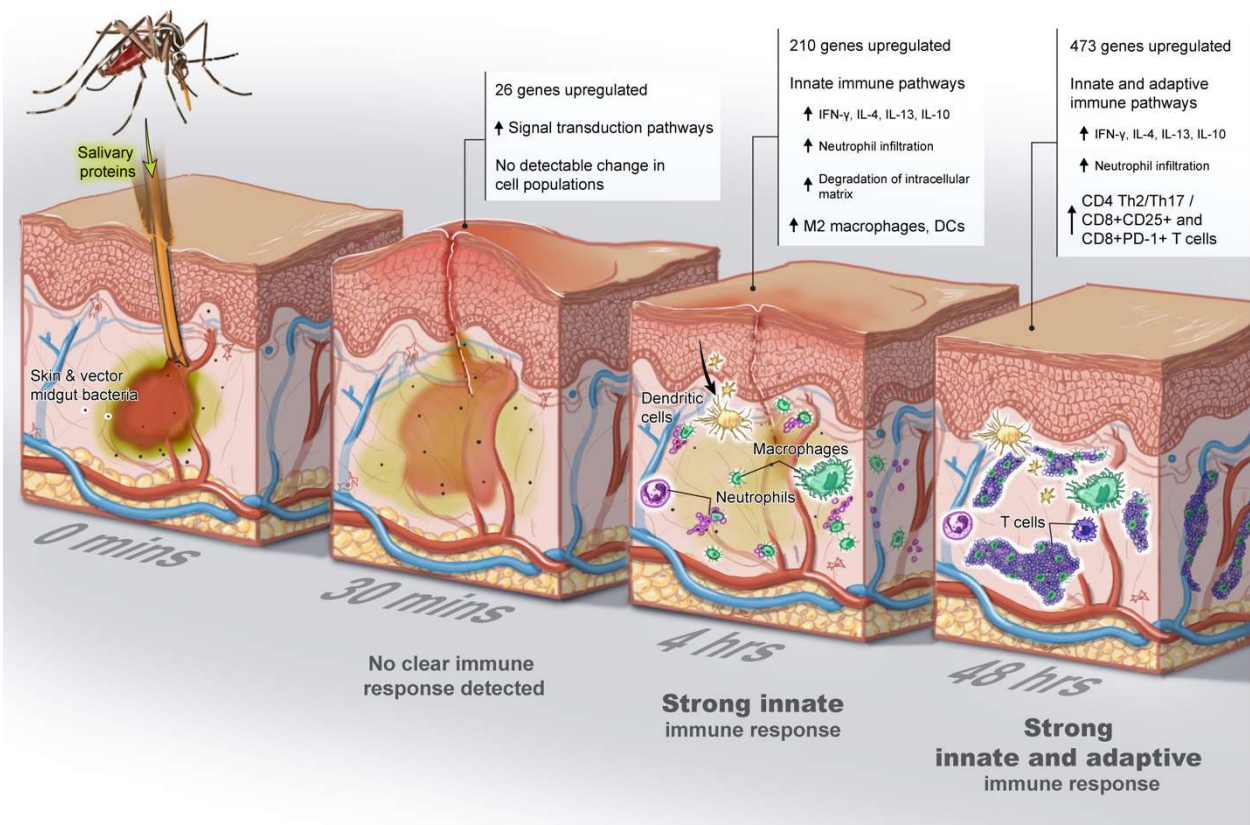
Graphical Abstract

Panel shows evolution of the human skin response to *Aedes aegypti* bites over time.

Introduction

With one million deaths every year, vector-borne diseases remain a major health problem worldwide[1]. In particular, arboviruses are of particular concern given a global distribution and a burden of nearly half a billion infections[2]. Several clinically significant arboviruses such as yellow fever (YFV), dengue (DENV), chikungunya (CHIKV), and Zika (ZIKV) viruses are all transmitted by *Aedes spp.* mosquitoes. These vectors are abundant in tropical and subtropical areas, but current climate change and rapid urbanization are expanding their transmission potential and increasing the at-risk population[3].

Mosquitoes first acquire an arbovirus via insertion of their proboscis into the dermis of an infected host during a blood meal. The virus then replicates in midgut cells to later disseminate and reach the salivary glands (SG)[4]. During a subsequent blood meal, the infectious mosquito inoculates virus and insect-derived molecules, including salivary components, into the dermis of a new human host. The saliva from hematophagous mosquitoes is a cocktail of pharmacologically active molecules, some of which are anti-hemostatic, angiogenic, and immunomodulatory[5–7]. Over the last couple decades, several animal and *in vitro* studies demonstrated that inoculation of vector saliva, and/or concomitant blood-feeding by an arthropod, can immunomodulate the host antiviral response in the skin and periphery[7–10]. These perturbations result in altered cytokine production profiles [11–13], promotion of recruitment of infection-susceptible cells to the bite site[14,15], stimulation of autophagy activation[5], and an induction of neutrophil infiltration to the local inflammation site[15] amongst other consequences. Mosquito-inoculated DENV or ZIKV infection in macaques led to higher or delayed viremia compared to non-vector or needle inoculation routes[16,17]. With regard to clinical pathogenesis, mice inoculated with both Semliki Forest virus and mosquito saliva had higher loads of virus RNA in the skin, earlier brain dissemination, and more frequent lethal

84 outcomes than animals inoculated with virus alone[12]. Taken together, arthropod-mediated viral

85 infection leads to increased disease progression, viremia, and mortality[8,9]. Despite this robust

86 evidence from animal and *in vitro* studies, there are no translational studies on the human skin

87 response to mosquito bites, much less those in tropical areas. Individuals are continuously exposed

88 to mosquito bites, possibly shaping their immune responses to mosquito salivary proteins in

89 contrast to those intermittently or rarely exposed[18,19]. In order to examine the dermal and epidermal

90 innate and adaptive immune responses to *Ae. aegypti* saliva, we compared the immune responses

91 before and after *Ae. aegypti* bites in skin biopsies from 30 healthy Cambodian individuals living

92 in an area where *Ae. Aegypti* mosquitoes are prevalent. Our study provides information on the key

93 genes and cell populations involved in the human immune response at different time points after

94 the 'mosquito bite.'

95 **Results**

96 **Controlled *Aedes aegypti* bite challenge in healthy volunteers in Cambodia**

97 From October 2020 to January 2021, we enrolled 30 healthy Cambodian adults at Kampong Speu

98 District Referral Hospital in Chbar Mon, Cambodia. The study population comprised 13 females

99 and 17 males, all of whom were of Khmer (Cambodian) ethnicity (Supplementary Table 1). The

100 population was randomly divided in three groups to assess immune responses by different

101 technologies (Fig. 1). The median age was 32.5 years (IQR 22–35) and the primary occupations

102 were variable, although nearly half (14/30) were unemployed. In terms of mosquito exposure risk,

103 most participants reported living in a house (20/30), being middle income (25/30), having one to

104 two domestic water containers (22/30). Notably, most participants did not use larvicide (28/30) or

105 insecticide (19/30) in their homes. Only 10% (3/30) reported prior dengue infection, but all 30

106 participants were positive for dengue anti-NS1 antibodies. All participants had detectable IgG to

107 *Ae. aegypti* salivary gland extract (SGE) prior to mosquito feeding, and these levels were not

108 significantly different by age, gender, or 14 days after the mosquito feeding (Supplementary Figure

109 S1). One participant did not complete Day 14 follow-up and was considered lost to follow-up.

110 No unanticipated adverse events occurred with the biopsies or mosquito feedings.

111
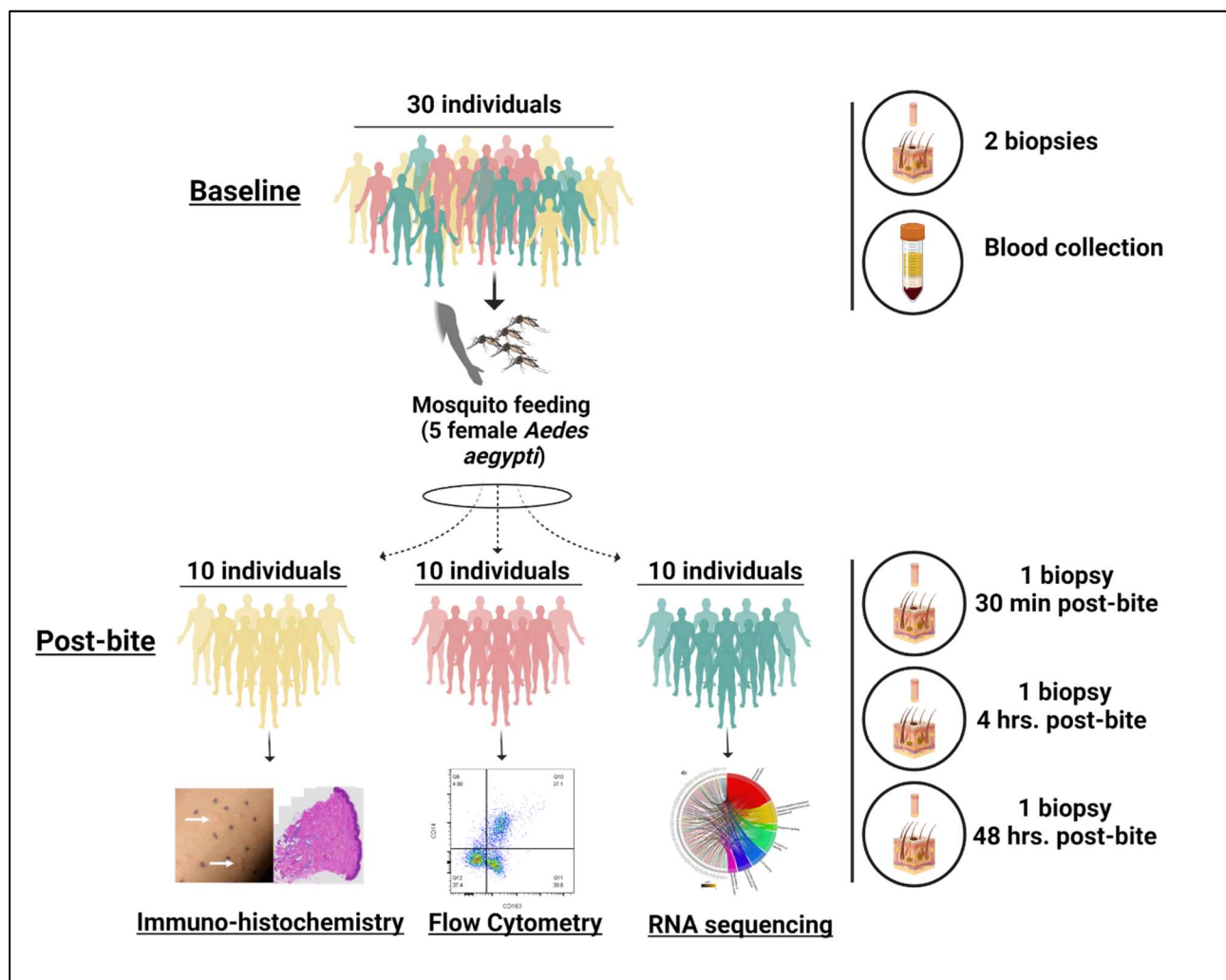
112 Figure 1. **Graphical Representation of Study Design.** Thirty Cambodian participants were

113 enrolled in the study. Each patient underwent a mosquito feeding (5 females *Aedes aegypti*) for

114 ten minutes. Each volunteer underwent a 3mm biopsy from a mosquito bite site at 30 minutes, 4

115 hours, and 48 hours. Distinct bite sites were biopsied at different time points. Additionally, two

116   3mm biopsies of normal skin (NSK) were taken from the opposite forearm. Blood was collected

117   to obtain serum.

Marked clinical changes occurred in the skin post-mosquito feeding

119   Exposure to five *Ae. aegypti* mosquitos resulted in 3 to 10 visible bite sites per volunteer. Upon

120   clinical observation, participants experienced erythema and swelling with a "bite size" reaction

121   that peaked at 15 minutes after feeding (Fig. 2a). The mean bite size of 4.9mm at 15 min after

122   feeding decreased to 4.7 mm at 30 minutes, to 2.7 mm at 4 hours and gradually decreased to 2.1mm

123   by 48 hours (Supplementary Table 1). Observation of representative histological sections shows

124   increased recruitment of cells to the dermis and epidermis at 48 hours post-bite (Fig. 2b,c). There

125   was no difference in bite size reaction by gender or age.
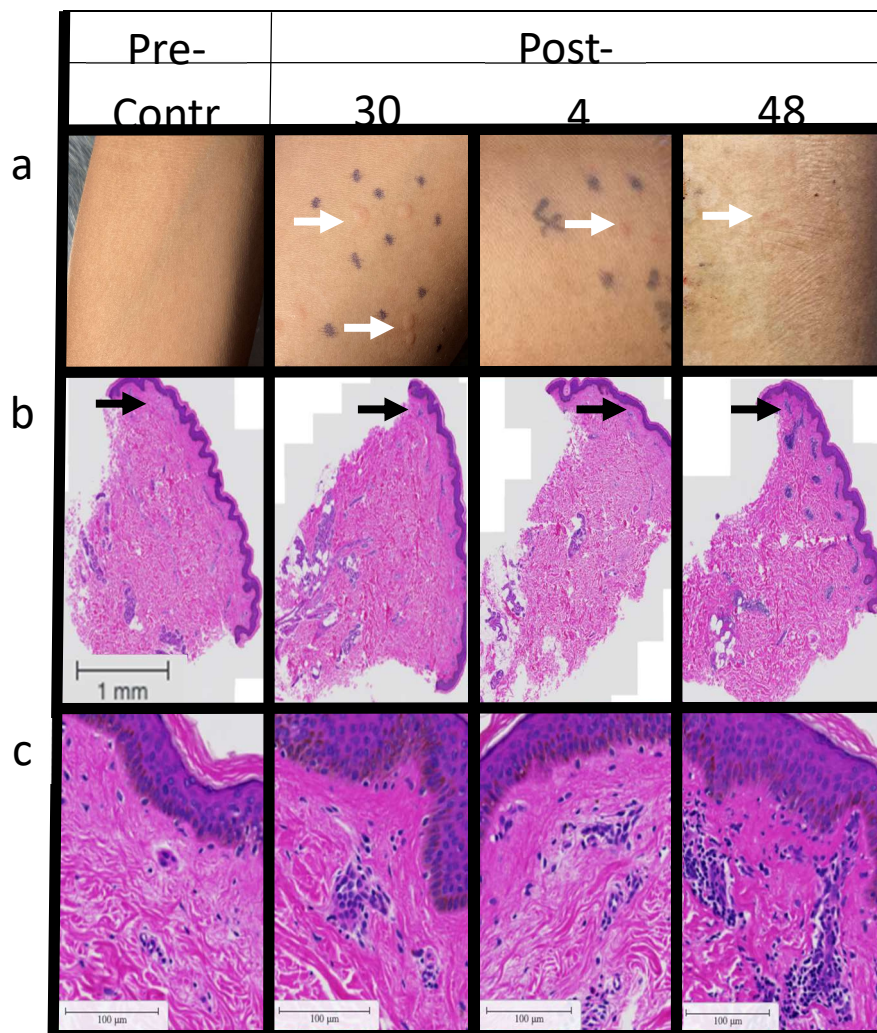
Figure 2. **Clinical observations of skin reaction pre- and post-bite on gross examination and H&E staining. a,** Skin immune responses to mosquito bites (left to right) normal skin (NSK), 30 minutes, 4 hours, and 48 hours after exposure to five *Ae. aegypti* mosquitos. **b,** Representative cross-sectional of 3mm punch biopsies H&E stained at (left to right) 0 hours, 30 minutes, 4 hours, and 48 hours after exposure to *Ae. aegypti* bites. Distinct bite sites were biopsied at different time points. Scale bar is 1 mm. Black arrows indicate area of infiltrate. **c,** Magnification of infiltrate indicated by black areas in B, scale bar 100μM.

**Changes in gene expression in *Aedes aegypti* bitten versus normal skin (NSK) evolved over 48 hours**

We extracted RNA and performed next generation sequencing on 40 skin biopsies from 10 participants (baseline normal skin (NSK) biopsy on the forearm, plus 3 follow-up biopsies each at 30 minutes, 4 hours, and 48 hours post *Ae. aegypti* bites on the contralateral arm). Principal Component (PC) analysis of *Ae. aegypti* bite site skin biopsies resulted in segregation of sample clusters based on the time the biopsy was taken (Fig. 3a), with PC1 and PC2 variances defining differences between NSK and 30 minutes versus 4 hours and 48 hours. While PC3 variance associated to the separation between biopsies taken at 4 hours and 48 hours, samples taken from NSK (pink circles) and 30 minutes after *Ae. aegypti* bites clustered in the same spatial area. At 4 hours post-bite, 6 of 10 samples occupied a distinct region (Fig. 3a, blue ellipse) from NSK, 30 minutes or 48 hours after *Ae. aegypti* bites. Similarly at 48 hours post-bite, 7 of 10 samples segregated into a discrete space (Fig. 3a, orange ellipse) compared to NSK, 30 minutes or 4 hours after *Ae. aegypti* bites. These data indicate that time post-bite rather than inter-individual differences drive unique patterns in gene expression. Differential analysis of RNA expression with a threshold of two-fold ($-1 < \log2FC > 1$; False discovery rate (FDR) < 0.05) over NSK biopsies resulted in 709 upregulated genes post-bite compared to 31 downregulated genes (Fig. 3b, red circles). At 30 minutes, 4 hours, and 48 hours after a mosquito bite, 26, 210 and 473 genes were upregulated over NSK, respectively (Fig. 3c, Supplementary Table 2). Conversely, one gene at 4 hours and 27 genes at 48 hours were downregulated after *Ae. aegypti* bites (Supplementary Table 2).

Upregulated genes at each time point were subjected to over-representation analysis (ORA) for enriched pathways using the Reactome database with an FDR cut off < 0.05. Four pathways related

158   to cell proliferation, cell growth and nuclear transcription were identified (FDR < 0.05) at 30

159   minutes after *Ae. aegypti* bites (Supplementary Table 3). At both 4 and 48 hours post-bite, the

160   immune nature of the host response to *Ae. aegypti* bites was evident via the revealed pathways

161   (Fig. 3d, Supplementary Table 3). At 4 hours post-bite, pathways such as "neutrophil

162   degranulation", "Interleukin-4 and Interleukin-13 signaling", "Interleukin-10 signaling",

163   "Interferon-γ signaling" "Chemokine receptors bind chemokines" and "Immunoregulatory

164   interactions between a Lymphoid and a non-Lymphoid cell" (Fig. 3d, upper chord) were

165   significantly overrepresented and maintained until 48 hours post-bite (Fig. 3d, lower chord).

166   Unique pathways discovered at 4 hours post-bite were related to "degradation of extracellular

167   matrix" (Fig 3d, upper chord) while "antimicrobial peptides" pathway and "adaptive immune

168   system processes" were present at 48 hours post-bite including "TCR signaling", "Co-stimulation

169   by the CD28 family", "PD-1 signaling", "MHC class II antigen presentation" (Fig. 3d, lower

170   chord). A heatmap with differentially expressed genes (DEG) under an FDR cutoff < 0.05 and

171   log2FC >1 in at least one timepoint was assembled (Supplementary Figure S2, Supplementary

172   Table 4), showing the dynamics of DE expression throughout the three timepoints. Fig. 3e shows

173   DEG driving the common pathways found on Fig. 3d.

174   Overall, few DEG genes were detected at 30 minutes post-bite compared to NSK biopsies. The

175   main upregulated gene FOSB (up 18.8x) is one of the transcription factors of the FOS family

176   proteins that regulate cell proliferation and differentiation (Supplementary Table 2). As the

177   reaction progresses over time, gene expression increased towards neutrophil recruitment followed

178   by signaling of both Th1, Th2, and regulatory pathways. The five most regulated genes at 4 hours

179   compared to NSK are KRT6C (related to keratinization; up 80.8x), CXCL8 (neutrophil-attracting

180   chemokine IL-8 up 75.0x), TNIP3 (inhibitor of NF-kappa-B activation; up 59.3x), IL-20

181   (stimulates keratinocyte proliferation and differentiation; up 59.1x) and IL-1B (pro-inflammatory

182   cytokine; up 45.7x) (Supplementary Table 2). The immune response evolved at 48 hours post-bite

183   to include adaptive immune response pathways related to T-cell priming. The five top genes at 48

184   hours are KRT6C (related to keratinization; up 59.6x), DEFB4A (an antimicrobial peptide; up

185   32.7x), GZMB (Granzyme B, up 21.1x), TCL1A (proliferation of T and B cells; up 20.3x) and

186   CCL18 (chemokine associated with associated with TH2 responses; up 18.5x).

187
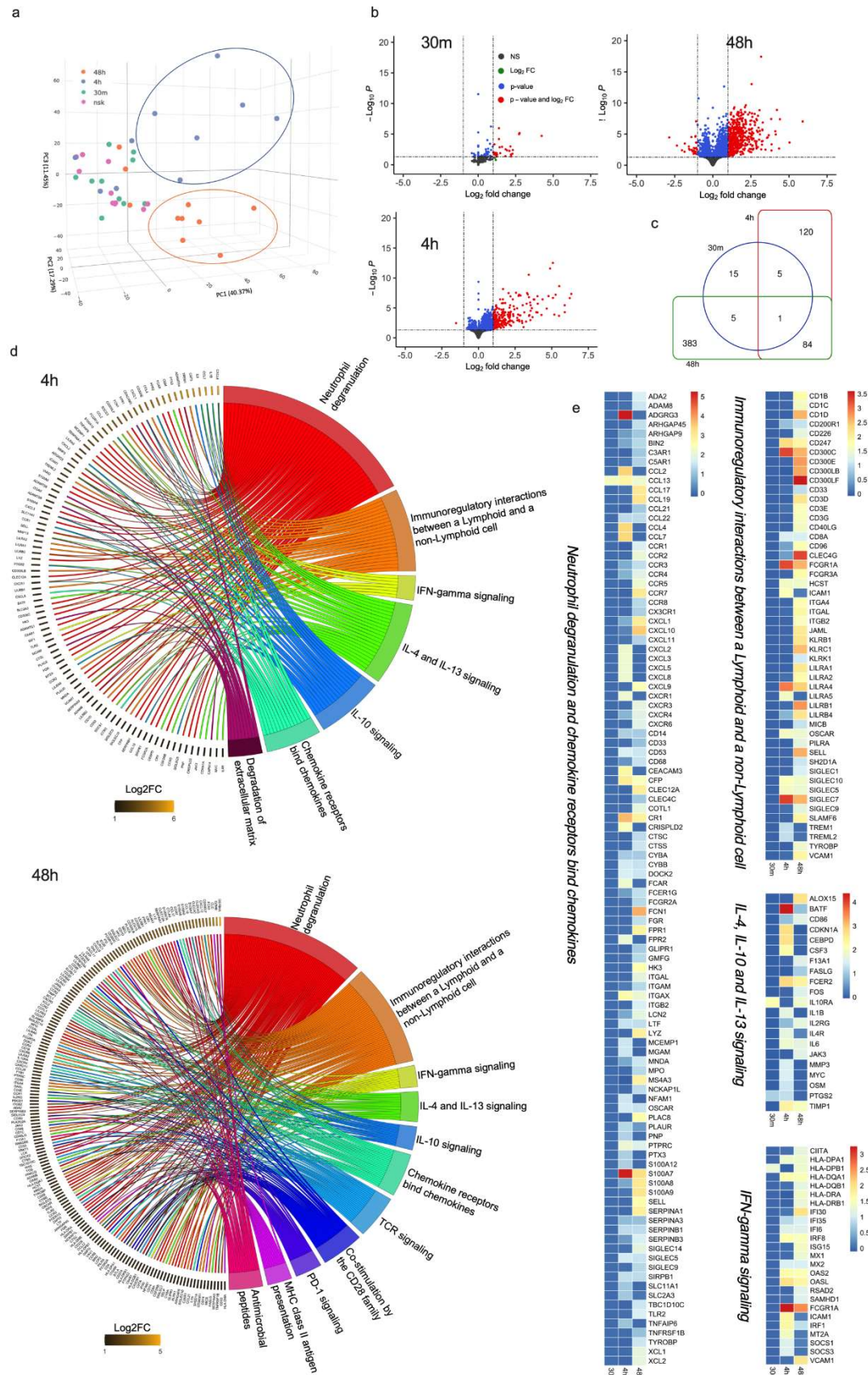
188 Figure 3. **Differential expression gene (DEG) and pathway analysis induced by *Aedes aegypti***

189 **mosquito bites over time. a,** 3D principal component analysis showing clustering of individual

190 biopsies taken at 30 minutes (green dots), 4 hours (blue dots), 48 hours (orange dots) post-bite or

191 normal skin (NSK; pink dots). Blue ellipse indicates clustering at 4 hours, while orange ellipse at

192 48 hours. **b,** Volcano plot comparing DEG from skin biopsies post-bite with NSK (significant

193 genes with -1 < log2FC >1 and FDR < 0.05 are shown in red). **c,** Venn diagram summarizing the

194 relationships between significantly upregulated genes over NSK (log2FC >1 and FDR < 0.05) and

195 time post-bite. **d,** Chord plot shows significantly upregulated genes at 4 hours and 48 hours post-

196 bite over NSK (left side of chord plot) and overrepresented pathways (right side of chord plot).

197 Outer left ring shows genes and color range displays log2 fold change (left, key at bottom) or

198 Reactome terms (outer right ring). Chords connect gene names with Reactome term pathways. **e,**

199 Heatmap (scaled to log2FC) displaying a list of DEGs based on the common pathways

200 overrepresented at 4- and 48-hours post-bite.

201

202 **Early innate immune response in the skin is characterized by increased proportions of DCs**

203 **and M2 macrophages and a decreased proportion of NK cells**

204 To confirm and extend the gene expression analysis, dissociated cells from NSK and skin biopsies

205 taken at 30 minutes and 4 hours after exposure to mosquitos, were characterized for innate and

206 adaptive immune subsets by flow cytometry (Supplementary Figure S3, Supplementary Table 5).

207 No significant changes in cell populations were detected between NSK and 30 minutes post-bite,

208 mirroring the transcriptomic analysis of DEG. At 4 hours post-bite, the proportion of dendritic

209 cells (DC), and M2 macrophages increased, while the proportion of mast cells, natural killer (NK)

210 and T-cells decreased, when compared to NSK and 30 minutes post-bite (Fig. 4a). The frequencies

211   of DC subsets increased at 4 hours post-bite compared to NSK and 30 minutes (Fig. 4 b-e). Within

212   the DC subsets, Langerhans cells (CD45+CD3-CD207+) increased at 4 hours compared to NSK

213   (Fig. 4d). A decreasing, though non-significant trend in the NK cell population frequency was

214   observed over time (Fig. 4f). Regarding the macrophage population, M2-skewed macrophages

215   (CD45+CD14+CD163+) frequency increased after 4 hours post-bite as well as their expression of

216   activation markers (CD16/CD69) compared to NSK and 30 minutes (Fig. 4 h-j). Frequencies of

217   activated M2 macrophages, and frequency of Langerhans cells positively correlated with clinically

218   observed changes in bite size at 30 minutes (Supplementary Figure S4 a, b). In order to evaluate if

219   changes in total leukocytes (CD45$^+$) were affecting the reported frequencies, we analysed the

220   changes of the innate cell population within total live cells. Here, similar results were observed

221   (Supplementary Figure S5). Unfortunately, we did not include specific neutrophil markers to our

222   flow cytometry panels. Alternatively, when we gated on CD45+CD11b+CD14-CD56-CD117-

223   cells, that comprises mostly of neutrophils, we detect a significant "neutrophils" accumulation at

224   4 hours post-bite compared to NSK (Supplementary Figure S6). The relative proportion of CD4$^+$

225   and CD8$^+$ T cells did not change over time. Taken together, the results suggest that immune cell

226   infiltration and migration occurs in local skin tissue within 4 hours post-bite and is characterized

227   by increased frequencies of DCs, M2 macrophages and neutrophils, but decreased frequencies of

228   NK cells.

229
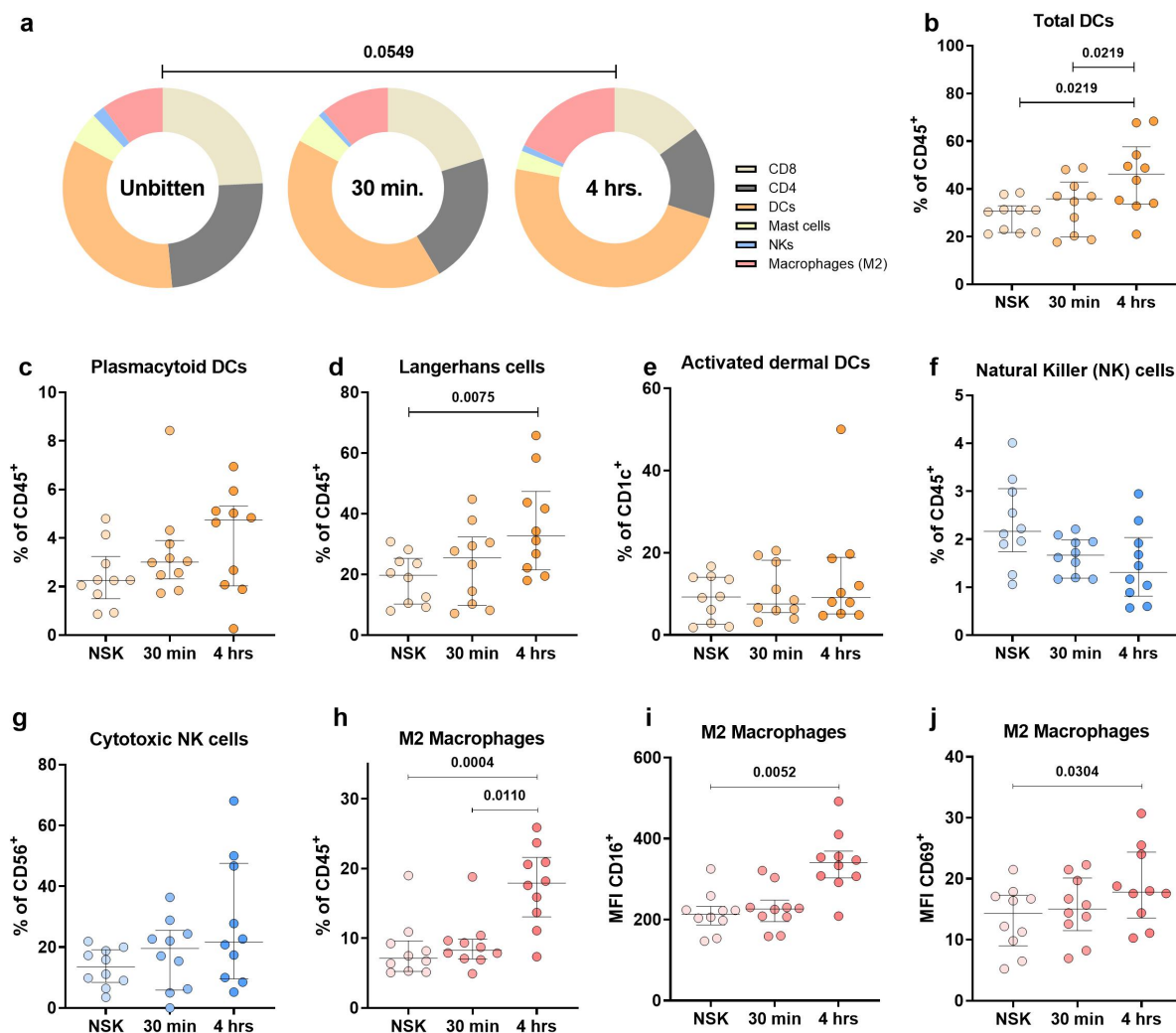
Figure 4. **Early innate immune responses in the skin are characterized by increased proportions of DCs and M2 macrophages, and a decreased proportion of NK cells at 4 hours post-bite**. **a,** Pie charts showing changes in the frequencies of skin immune cells during early innate immune response to mosquito bite at 30 minutes and 4 hours after exposure. Frequencies are reported as percentages of total leukocytes (CD45$^+$) **b,** total frequency of dendritic cells calculated as the sum of Langerhans (CD207$^+$), dermal (CD1c$^+$) and plasmacytoid (CD123$^+$) DCs. **c,d,** Frequency of plasmacytoid dendritic cells and Langerhans cells populations reported as percentage of total CD45$^+$ cells shows significant increase of the later, at 4 hours post mosquito

238   bites. **e,** Frequency of activated dermal DCs (CD1c$^+$CD69$^+$) from the total dermal DCs population

239   (CD1$^+$). **f,** Frequency of NK cells (CD56) reported as percentage of total CD45+ cells. **g,**

240   Frequency of cytotoxic NK cells (CD56+CD16+) as percentage of total NK cells. **h-j**, Frequency

241   of M2 macrophages and MFI of their expressed activation markers CD16 and CD69. Statistical

242   analysis were performed with Chi-square test (**a**) and Friedman + Dunn's multiple comparisons

243   test (**b-j**). Bars indicate median and interquartile range. N=10

244

245   **Changes in the T cell compartment are observable at 48 hours after mosquito 'bite'**

246   Changes in skin T cell populations were assessed using NSK and biopsies taken at 48 hours post-

247   bite. We found that the frequency of CD8+CD25+ and CD8+PD-1+ T-cells increased at 48 hours

248   post-bite, compared to the NSK (Fig. 5a). Frequencies of CD8+ T cells correlated inversely with

249   the bite size at 48 hours (Supplementary Figure S4c). The frequency of effector memory cells re-

250   expressing CD45RA (T$_{EMRA}$) CD8 T cells (CD8+CCR7-CD45RA+) decreased at 48 hours (Fig.

251   5b). In the CD4+ T cell compartment, we observed a decrease in the frequency of Th1/Th17

252   (CD4+CCR4-CXCR3+) cells at 48h compared to NSK and an increase in the frequency of

253   Th2/Th17 (CD4+CCR4+CXCR3-) cells (Fig. 5c). The frequency of CD4+ effector memory T

254   cells (T$_{EM}$) (CD4+CCR7-CD45RA-) increased at 48 hours compared to NSK, while the frequency

255   of T$_{EMRA}$ cells (CD4+CCR7-CD45RA+) decreased (Fig. 5d). Results were similar when analyzing

256   the changes of T cell frequencies within all live cells (Supplementary Figure S7). Interestingly,

257   no changes were observed in the frequencies of skin-resident CD4 (CD4+CD103+CLA+) or CD8

258   (CD8+CD103+CLA+) T cells (Supplementary Figure S8). At 48 hours post-bite, these results

259   show an increase in the frequency of activated CD8 T cells in addition to a shift from Th1/Th17

260   towards Th2/Th17 polarization of CD4 T cells.
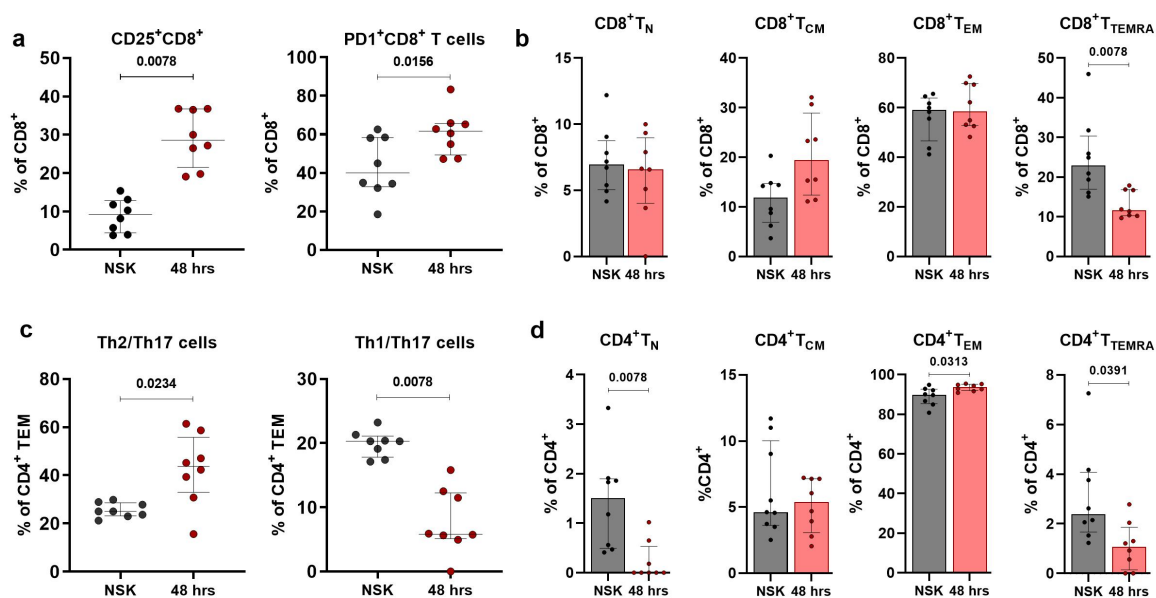
Figure 5. **Changes in the T cell compartment are observable at 48 hours after mosquito exposure. CD8 T cells exhibit a high activation phenotype, while CD4 T effector memory cells shift from a Th1/Th17 phenotype to a Th2/Th17 phenotype. a,** Increased frequency of CD25+ and PD1+ CD8 T cells at 48 hours post mosquito exposure. **b,** Frequencies of CD8 T cells naive (CCR7+CD45RA+), central memory (CCR7+CD45RA-), effector memory (CCR7-CD45RA-) and TEMRA (CCR7-CD54RA+) frequencies. **c,** decreased Th1/Th17 and increased Th2/Th17 effector memory CD4 T cell compartment at 48 hours. **d,** CD4 T cells naive (CCR7+CD45RA+), central memory (CCR7+CD45RA-), effector memory (CCR7-CD45RA-) and TEMRA (CCR7-CD54RA+) frequencies. Statistical analysis of 8 samples dedicated to this time point was performed with Wilcoxon signed-rank test. Bars indicate median and interquartile range.

274 **"Bitten" human skin cells stimulated by *Aedes aegypti* saliva produce significantly less pro-**

275 **inflammatory cytokines**

276 Next, we sought to assess if *Ae. aegypti* saliva impacted cytokine production by skin cells taken

277 48 hours post-bite. We measured pro- and anti-inflammatory cytokines released into the media

278 after a stimulation assay with and without *Ae. aegypti* SGE. Both NSK and SGE-treated cells

279 showed low secretion of cytokines in the media (Supplementary Figure S9). However, we

280 observed a significant reduction in the levels of Interleukin 2 (IL-2) and Interferon gamma (IFN-

281 γ) in the cells treated with both SGE and PMA/Ionomycin compared to the cells treated with

282 PMA/Ionomycin alone (Fig. 6, Supplementary Figure S9). The levels of other pro-inflammatory

283 cytokines like TNF-α, IL-17A and IL-17F showed no significant differences (Fig. 6). Similarly,

284 no differences in the regulatory cytokine IL-10 was observed (Fig. 6). This data suggests that SGE

285 has a dampening effect on the production of pro-inflammatory cytokines IL-2 and IFN-γ under

286 stimulatory conditions in "bitten" human skin cells.

287
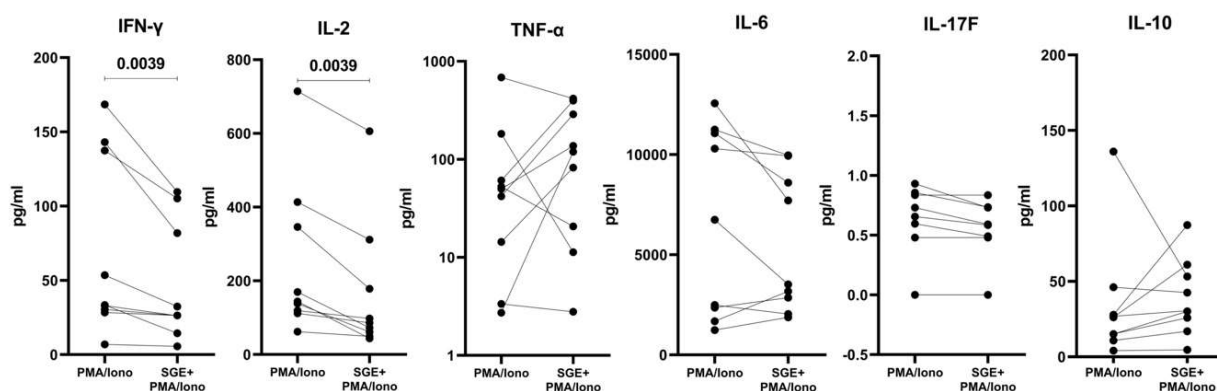
288 Figure 6. **Human skin cells obtained from *Ae. aegypti* bitten skin stimulated by *Ae. aegypti***

289 **salivary gland extract (SGE) produce significantly less pro-inflammatory cytokines (IL-2**

290 **and IFN-γ).** Cytokine production measured in skin cell culture supernatant after treatment with

291 PMA/Ionomycin in the presence or absence of SGE. Skin dissociated cells were seeded on round

292 bottom 96-well plates (50.000 cells/well) and treated with SGE (10 µg/mL) or PBS for 24 hours.

293 Cells were stimulated with PMA (0.1µg/mL) and Ionomycin (1µg/mL) or left unstimulated for the

294 last 6 hours of the culture. Statistical analysis was performed with Wilcoxon signed-rank test. N=9

295 individuals.

296

297 **Discussion**

298 Arboviruses enter the host through the skin when the arthropod injects its saliva and other

299 components into the dermis while taking a bloodmeal. Data from mice and macaques suggest that

300 the unique dual presence of virus and saliva orchestrates an immunological cascade of events that

301 influence the establishment and course of infection[12,16,17]. To translate these findings to humans,

302 the current study assessed the dynamics of the cutaneous immune response to arthropod bites from

303 a clinically relevant vector, the *Ae. aegypti* mosquito, in humans from arboviral-endemic areas

304 with lifelong exposure to *Aedes* mosquitos. At 4 hours post-bite, we observed upregulation of

305 genes involved in neutrophil recruitment and increased frequencies of dendritic cells and M2

306 macrophages. As the immune response progressed over two days, we observed an increased

307 frequency of activated, PD-1+CD8+ T cells, a polarization towards Th2/Th17 CD4+ T-cells, and

308 upregulation of IL-10, IL-4, and IL-13 and IFN-γ related pathways. Interestingly, these human

309 skin cells post-bite produced less pro-inflammatory cytokines when stimulated by Ae. aegypti

310 SGE.

311 A mosquito 'bite' results in minor tissue damage by the proboscis, injection of mosquito saliva

312 into the skin, and introduction of both mosquito and host microbiota into the skin. In this study,

313   we did not parse out the separate impact of each process on the skin immune response. Alterations

314   in skin immunity due to injury from the punch biopsy itself were mitigated by ensuring biopsy

315   sites were at least 10 to 20 mm away from one another and were not taken directly at the site of

316   the needle administration of subcutaneous lidocaine. The effect of local anesthetic was mitigated

317   by the case-control design that each person's anesthetized, bitten skin was compared to

318   anesthetized, unbitten skin, presumably negating any immediate cutaneous immune effects

319   attributed to lidocaine, for which the literature is sparse.

320   Mosquito bites cause a local cutaneous reaction with wheal and flare manifestation[20,21].

321   Concordantly, the bite size reaction peaked after 15 minutes post-bite in this endemic study

322   population. Few changes were detected in gene expression or influx and activation of neutrophils,

323   dendritic cells subsets and macrophages at the 30 minutes post-bite time point. Upregulated genes

324   were related to top-level processes such as signal transduction. We did not design this study to

325   assess the role of pre-stored immune mediators such as histamine (and others) in the development

326   of edema and their modulation in the immune response. Indeed, mosquito bites can activate

327   cutaneous mast cells, which are prominent histamine-storing cells, and induce their degranulation.

328   The release of histamine and other mediators leads to vasodilation, fluid accumulation at the bite

329   site, and neutrophil influx, which were all ultimately observed here[20,21].

330   As the immune reaction progressed, the mosquito 'bite' induced degradation of the extracellular

331   matrix (ECM), and a strong influx of dendritic cells and macrophages at 4 hours post-bite,

332   consistent with previous animal observations[22]. We observed several disintegrin and

333   metalloprotease with thrombospondin type I motifs (ADAMTS) were upregulated, mostly at 4

334   hours post-bite, that can be associated with ECM degradation. Similarly, granzyme B (GZMB)

335   upregulated at 48 hours, despite its effects on inducing inflammation it may also be involved in

336   ECM degradation using as substrate fibronectin, vitronectin, laminin and others[23,24]. Saliva from

337   blood-feeding arthropods contains anti-hemostatic proteins that prevent coagulation and promote

338   vasodilation, leading to increased leukocyte trafficking[20,25]. These processes – extracellular matrix

339   degradation and vasodilation – can facilitate viral infection by disrupting vascular functions, as is

340   the case of sialokinin, a mosquito salivary protein that hinders endothelial barrier integrity[26]. In

341   addition, elevated leukocyte trafficking can facilitate viral replication by augmenting the

342   proportion of susceptible cells to the local inoculation site[12,15,26]. Indeed, as most leukocyte subsets

343   are permissive to infection by most arboviruses, they play a dual role in the infection process: both

344   as replication targets/dissemination vehicles and as the first line of defense. Indeed, the increased

345   presence of activated M2 macrophages and dendritic cells at 4 hours post-bite highlight the cellular

346   trafficking role initiated by 'the bite' that can ultimately result in viral dissemination. The observed

347   increase in CD163+CD14+ cells at 4 hours is what we believe to be an initiation of the

348   differentiation of monocytes and macrophages into M2-skewed macrophages given that full

349   macrophage polarization does not occur as early as 4 hours [27–29]. Upregulated chemokines such as

350   CCL2 and CCL7, attracting mainly monocytes, DCs and T cell, may be participating in this

351   recruitment[30]. M2-polarized macrophages produce anti-inflammatory cytokines, mediate wound

352   healing processes, and support Th2 responses [31]. Moreover, activation of M2 macrophages

353   positively correlated with the bite size in our study. Upon stimulation, DCs upregulated CD69,

354   preventing them from exiting the tissue and improving the likelihood of antigen internalization.

355   Subsequent CD69 downregulation promotes Sphingosine-1-Phosphate (S1P1) leading to DC

356   migration to the lymph nodes[32]. The CD69-S1P1 mechanism of cell retention in tissue is also well-

357   described for resident T cells,[33] whose role in saliva-mediated immunity is not yet known.

358   *Ae. aegypti* mosquito saliva has a clear impact on neutrophil influx and degranulation. Two

359   recently identified *Ae. aegypti* salivary proteins (NeSt1 and AgBr1) that attract and stimulate

360   neutrophils at the 'bite site,' changing the immune microenvironment and leading to increased

361   early ZIKV replication and enhanced pathogenesis[14,15]. Here, at 4 hours post-bite, chemokines

362   CXCL2, CXCL3, CXCL5, and especially CXCL8, plus the cytokine IL-1B were upregulated

363   returning to levels comparable to NSK at 48 hours post-bite. CXCL2-5 chemokines are responsible

364   for attracting neutrophils and exhibiting angiogenic properties[34]. Pro-inflammatory responses

365   through inflammasome activation and IL-1B production can trigger a sustained neutrophilic

366   response[12]. Microbiota egested during infected sand fly bites contributed to IL-1B production[35],

367   but we were unable to assess the effects attributed to vector microbiota in this study. On the other

368   hand, IL-20 was upregulated at 4 hours post-bite. IL-20 is most active at epithelial sites

369   downregulating IL-1B resulting in deactivation of neutrophil functions such as phagocytosis,

370   granule exocytosis, and migration[36,37]. Increased gene expression for neutrophil recruitment and

371   degranulation at 4 hours post-bite in our Cambodian study population further supports the timing

372   of neutrophil influx seen 3 hours post-bite in bite-experienced C57BL/6 immunocompetent mice[12].

373   How the timing of neutrophil influx would differ in a bite-naïve population is a question that

374   remains to be answered as none of the participants would be considered naïve. Moreover, studies

375   of 'infected bites' would clarify the role of both 'neutrophil influx' and extracellular matrix

376   degradation in facilitating pathogen establishment[12,38], but currently approved human challenge

377   models deliver DENV via needle inoculation, not via mosquito bite[39].

378   As the immune response transitioned from innate to adaptive, a strong T-cell signature emerged at

379   4 and 48 hours emerged after the mosquito 'bite'. CD8+ T cell activation was confirmed by

380   increased expression of CD25, an early activation marker. Skin CD8+ T cells also upregulate PD-

381   1 expression, an immune-checkpoint receptor that is induced by yet can also inhibit T cell

382   activation. PD-1 primarily inhibits effector function acquisition by T cells, the loss of sensitivity

383   after T cell receptor signaling and modulation of cytotoxicity, and inhibition of TNF-α and IL-2

384   production along with T-cell expansion[40,41]. Interestingly, highly activated CD8+ cells have been

385   observed in skin from dengue shock syndrome patients[42,43]. Here at 4 and 48 hours post-bite, CD4+

386   T cells had a skewed phenotype to Th2-like cells and IL-10, IL-13, and IL-4 related pathways were

387   upregulated compared to NSK. CCL18, upregulated at 48 hours post-bite, can be expressed by M2

388   macrophages and is linked to increased IL-4, IL-10, and IL-13, especially in the presence of

389   histamine[44]. Indeed, initial animal experiments also pointed to a Th2-mediated allergic

390   inflammatory response following mosquito bites or inoculation with SGE[13]. In case of arbovirus

391   infection, virus will replicate locally in the skin, and the local skin immune responses will direct

392   the course of the systemic host immune response. At 48 hours post-bite, arboviruses will also have

393   disseminated to draining lymph nodes[45]; hence , the contribution of the localized Th2 polarization

394   at this time point on disease outcome remains to be determined.

395   At 48 hours post-bite, other upregulated genes such as CD28, ICOS, and CTLA-4 further suggest

396   a regulatory role of the CD4+ compartment in controlling the local immune responses to *Ae.*

397   *aegypti* saliva. Th2 polarization is essential to avoid excessive collateral damage from an

398   exacerbated pro-inflammatory response, especially in a situation where the skin immune cells are

399   repeatedly exposed to the same type of insult, as is the case with individuals living in tropical areas

400   of mosquito abundance. Blood DC antigen-2 (CLEC4C), upregulated at 48h compared to NSK, is

401   thought to signal through BDCA-2 to inhibit activation of the NF-κB pathway, inhibit production

402   of type I IFNs, and block TRAIL-mediated cytotoxic activity[46]. This may represent a possible

403   mechanism that differentiates chronically exposed individuals compared to naïve individuals.

404 To consider other potential mechanisms that immunomodulate the microenvironment, we noted

405 increased expression at 48 hours post-bite of ficolin-1 (FCN1), a complement lectin pathway

406 protein that may bind and opsonize mosquito microbiota or salivary components, then activate the

407 complement pathway[47]. Another C-type lectin receptor LSECtin (CLEC4G, increased at 48 hours

408 compared to NSK) negatively regulates T cell-mediated immunity and may be also linked to

409 apoptotic cell clearance by macrophages[48]. Of note, the upregulation of CXCL10 chemokine and

410 its receptor CXCR3 are linked to their major roles of inflammatory reactions, T cell migration, and

411 IFN-γ in the saliva-mediated process[49]. Besides chemokines, the top expressed molecule was an

412 antimicrobial peptide hBD-2 (DEFB4A), produced by neutrophils and keratinocytes. DEFB4A is

413 a marker of inflammation absent in normal skin and responsible for recruitment of memory T cells,

414 immature DCs, mast cells and neutrophils[50,51].

415 In this study, the presence of mosquito saliva inhibited pro-inflammatory cytokine production by

416 'bitten' human skin cells after *in vitro* re-stimulation with SGE. One consideration is that we used

417 SGE, rather than mosquito saliva as forced salivation did not provide sufficient material, but our

418 preparations minimize the cellular components of the salivary glands. The cytokine-dampening

419 effect may partly result from the interaction between salivary components and key checkpoints on

420 different signaling pathways. One example includes the salivary protein LTRIN known to interfere

421 with the Nf-kB pathway by binding to LTβR, thus hindering its dimerization and leading to

422 decreased production of inflammatory cytokines[11]. On the other hand, skin immune tolerance to

423 constant mosquito exposure may also explain the reducing effect of SGE on cytokine production

424 as seen here in our bite-experienced participants[12,19,52].

425 Our results refine and extend the knowledge obtained from mouse models of mosquito biting. For

426 example, in mouse models, increased frequencies of dendritic cells, total macrophages and

427   neutrophils have been detected after mosquito bites [21,53,54]. In our human participants, we also

428   observe an increase in the frequency of these cells, indicating that the mouse models of mosquito

429   biting recapitulate the early innate events in human skin. However, we expand these data by

430   showing that the observed increased frequencies are due to increases in M2-like macrophages,

431   which are activated, and increases in Langerhans cells at 4 hours post-bite in our human

432   participants. Additionally, we substantially increased our knowledge on human T cell responses

433   to mosquito saliva by observing CD8 T cells exhibiting a high activation phenotype, while CD4 T

434   effector memory cells shift from a Th1/Th17 phenotype to a Th2/Th17 phenotype 48 hours post-

435   bite. Saliva or salivary proteins from ticks and sand flies have shown ability to inhibit proliferation

436   of both murine and human cells.[55,56] We here confirm the inhibitory effects of SGE to skin cells

437   recruited during a mosquito bite. Nevertheless, as previously showed in individuals from an

438   endemic area of leishmaniasis,[57] the immune responses to saliva of arthropods also triggers a pro-

439   inflammatory response highlighted by the upregulation of pathways related to interferon genes.

440   This mix of anti- and pro-inflammatory responses need to be further evaluated in animal models

441   of mosquito bite exposure as well as clinical field settings.

442   With the current rise of vector-borne diseases around the world, future clinical development of

443   vector-targeted strategies for both known and unknow vector-borne diseases will require a

444   fundamental understanding of how vector saliva modulates the cutaneous immune response of

445   humans. Translational studies, such as the one presented here, significantly expand our current

446   knowledge on human skin immunity and the immune response orchestrated by a 'mosquito bite'.

447   These newly identified genes, cell types, and processes of human cutaneous immunity can be

448   leveraged in the development of vector-targeted vaccine candidates or novel therapeutics such as

449   those targeting the reversibility of functional macrophage polarization or chemokine blockades

450 that may have application in other inflammatory disorders[58]com. Such new pathogen-agnostic

451 strategies have shown promising results in recent years from mosquito saliva-based vaccinations

452 to topical applications like imiquimod post-bite that activated skin macrophages in order to limit

453 pan-viral activity[59–62]. Building on these findings, the next generation of countermeasures against

454 vector-borne disease will require nuanced and comprehensive understanding of skin immunity to

455 both pathogen and vector saliva alike.

456

Materials and methods

Study Enrollment and Procedures

459 From October 2020 to January 2021, we enrolled thirty Cambodian adults at Kampong Speu

460 District Referral Hospital. Eligible participants were healthy adults between the ages of 18 and 45

461 years old who agreed not to use topical or oral antihistamines or steroids for the duration of the

462 study. Participants were excluded if they were pregnant or reported a history of severe allergic

463 reaction to mosquito or other insect bites, use of medications that affect blood clotting, or history

464 of significant scarring such as keloid formation (full criteria found on

465 https://clinicaltrials.gov/ct2/show/NCT04350905). All participants provided written informed

466 consent before enrollment, and the study was conducted in accordance with the provisions of the

467 Declaration of Helsinki and Good Clinical Practice guidelines.

468 On Day 0, five starved uninfected *Ae. aegypti* female mosquitos were selected from a mosquito

469 colony dedicated to human feeding studies in the Malaria and Vector Research Laboratory at the

470 National Center for Parasitology, Entomology and Malaria Control. Mosquitos fed through the

471 disposable mesh of a feeding device placed on participants' ventral forearm skin for 10 minutes.

472 Redness and swelling in millimeters were assessed immediately, 15 minutes, 30 minutes, 4 hours

473 and 48 hours after feeding. Redness and swelling were measured in millimeters at 15 minutes, 30

474 minutes, and 4 hours.

475 A total of five 3-mm skin punch biopsies were performed on each individual: one biopsy from

476 bitten skin per time point (30 minutes, 4 hours, and about 48 hours after feeding is completed) for

477 a total of three 'bitten' biopsies, and two from NSK collected at baseline. Biopsy sites were

478 selected based on the 3 bite sites with the largest diameters at 30 minutes after feeding. We tattooed

479 the area surrounding those 3 bite sites with a permanent marker and randomly picked one of the

480 three distinct sites for 30 min, 4 hours and 48 hours biopsies. Less than 1cc of 0. 2% lidocaine

481 without epinephrine was delivered via 30-G needle each chosen 'bite' at the time of biopsy and 3-

482 mm biopsy was performed on 'bite' adjacent to needle puncture. For feasibility of skin sample

483 analysis, each participant was assigned to 1 of 3 technical modality cohorts: 1)

484 immunohistochemistry, 2) RNASeq, and 3) flow cytometry with ten people in each cohort.

485 Additionally, blood was collected for serological and cellular analyses at baseline and 14 days

486 after feeding.

487 ***Aedes aegypti* SGE preparation**

488 Salivary glands from *Ae. aegypti* were dissected and collected in 200µl of PBS 1x (1pairs/1µl of

489 PBS 1x) in Low protein binding centrifuge tubes. Homogenization was done in an Ultrasonic

490 SONIFIER® (BRANSON) for 30 seconds on each side of the tube. The homogenates were then

491 centrifuged at 25,000 × g at 4 °C for 3 minutes, and the supernatant was collected and quantified

492 using Pierce™ BCA Protein Assay Kit (ThermoFisher Scientific, Cat# 23225) in an xMark™

493 Microplate Spectrophotometer (BIO-RAD).

494 ***Aedes aegypti* salivary IgG enzyme-linked immunosorbent assays**

495 *Ae. aegypti* SGE was diluted to a concentration of 2 ug/ul in carbonate-bicarbonate buffer

496 (Millipore-Sigma) and used to coat 96-well Immulon 4x HB plates (Nunc) overnight at 4°C. Plates

497 were blocked in a solution of TBS 4 % Bovine serum albumin 0.025 % Tween 20 (Millipore-

498 Sigma). Each plate included sera (1:200 dilution) from all time points, a negative control (non-

499 reactive human sera to SGE), an internal control (a pool of positive sera to SGE with OD set to

500 0.25 at 450nm) and blank wells. The controls were chosen accordingly from a stored bank of

501 human sera, well-characterized by reactivity to the saliva of various vectors, at the Laboratory of

502 Malaria and Vector Research. Plate-to-plate normalization was done by multiplication of all OD

503 values by a correcting factor to achieve the preset internal control OD 0.25 at 450nm. Secondary

504 antibody [goat anti-human IgG alkaline phosphatase (1:10000 in blocking solution; Millipore-

505 Sigma). A solution of p-nitrophenylphosphate (Millipore-Sigma) was used as substrate and OD

506 measured at 450nm in arbitrary enzyme-linked immunosorbent assay (ELISA) units and reported

507 in arbitrary ELISA units after correction stated above.

508 **Dengue IgG enzyme-linked immunosorbent assays**

509 The PanBio® Dengue Indirect IgG ELISA (product code 01PE30) was performed according to

510 the manufacturer's instructions. Two microtiter plates were supplied, one containing stabilized

511 dengue-1 through dengue-4 (antigen plate) and the other containing either anti-human IgM or anti-

512 human IgG bound to separate wells (assay plate). Peroxidase-labeled anti-dengue virus

513 monoclonal antibody (125 μl/well) was added to the antigen plate to solubilize the antigens and

514 form antibody-antigen complexes. Concurrently, 100 μl of patient serum was diluted 1:100 in the

515 provided diluent and added to each well of the assay plate containing either bound anti-human IgM

516 or bound anti-human IgG, and human IgM or IgG in the patient's serum was captured. The plates

517 were incubated for 1 h at room temperature (antigen plate) or 37°C (assay plate); then the assay

518   plate was washed, and 100 μl of antibody-antigen complexes per well was transferred from the

519   antigen plate to the assay plate. These complexes were captured by dengue virus-specific IgM or

520   IgG during incubation for 1 h at 37°C. The plate was washed, and bound complexes were

521   visualized through the addition of 100 μl of tetramethylbenzidine substrate per well. After 10 min,

522   the reaction was stopped by the addition of 100 μl of 1 M phosphoric acid per well, and the strips

523   were read at 450 nm with a microtiter plate reader. Positivity was determined by comparison to

524   the IgM and IgG reference sera provided (cutoff calibrators). A positive sample was defined as

525   having a sample/calibrator absorbance ratio of ≥1.0, and a negative sample was defined as having

526   a ratio of <1.0.

527   **Formalin preservation and H&E staining of skin biopsies**

528   Biopsies were placed in 7ml prefilled 10% formalin vials (Azer Scientific) and stored at 4°C until

529   paraffin embedded. Unstained slides were cut from paraffin blocks and deparaffinized in xylene,

530   then hydrated through graded alcohols up to water, placed in Carazzi's hematoxylin, washed in

531   tap water, and put in one change 95% ethanol. Next, they were placed in eosin-phloxine solution

532   and then run through graded alcohols to xylene. After xylene, the stained slides were than a cover

533   slip was mounted using Permount Mounting Media (Fisher Scientific).

534   **RNA extraction, RNA-seq library preparation, sequencing and analysis.**

535   Biopsies were stored in DNA/RNA Shield (Zymo research) and kept in 4 °C until processing. Skin

536   was homogenized using 3mm zirconium beads (Biolink laboratories) and a Magnalyser bead

537   beater (Roche Diagnostics®). After homogenization total RNA was loaded at InnuPure® C16

538   touch (AnalitikJena) for magnetic separation of total RNA using an InnuPREP® RNA Kit–IPC16

539   (AnalitikJena). Quality of extractions was verified on a 4200 TapeStation (Agilent) and all samples

540   had RIN numbers above seven. RNA sequencing was performed by Novogene. Briefly, mRNA

541 was enriched by Poly (A) capture and RNA libraries were prepared using the NEBNext Ultra II

542 Directional RNA Library Prep Kit for Illumina (New England Biolabs) and sequenced on a

543 NovaSeq 6000 (Illumina) generating paired end reads at 150 bp length. After removing low quality

544 reads (Trimommatic 0.39)[63], mapping to the human genome (hg38; GCF_000001405.39) and

545 gene-level quantification were generated by RSEM 1.3.2[64], Bowtie 2-2.4.2[65] and SAMtools

546 1.11[66]. Normalization and differential gene expression (DGE) analysis were performed using

547 DESeq2 1.34.0[67], employing the variance stabilizing transformed function (VSN 3.62.0)[68] to the

548 count matrix, that was designed to account for paired samples enabling expression analyses with

549 normal skin samples from the same subject as reference. Approximate Posterior Estimation for

550 GLM (Apeglm 1.16.0) method was used to calculate fold change of DEGs[69]. DEGs were

551 considered significant if apeglm-estimated shrunken log2fold change was <1 or >1 and with a false

552 discovery rate <0.05 (Benjamini–Hochberg multiple testing correction method[70]). PlotPCA3D

553 0.0.1(twbattaglia/btools) was used to generate tri-dimensional principal component analysis plots

554 on DESeq2. EnhancedVolcano 1.12.0 was used to generate volcano plots[71]. GOplot 1.0.[72] was

555 used to generate chord plots using data obtained from packages clusterProfiler 4.2.0[73] and

556 ReactomePA 1.38.0[74]. Pathways with a Benjamini–Hochberg corrected P value <0.05 and were

557 considered as enriched, selected pathways were mapped on chord plots[70]. Heatmaps were prepared

558 using package pheatmap 1.0.12.[75] and dendsort 0.3.4[76]. All DEG analyses were performed using

559 R 4.1.0[77].

560 **Skin biopsy dissociation**

561 Biopsies were transported in RPMI media (Sigma-Aldrich) at 4 °C. Whole skin dissociation kit

562 (Miltenyi®) was used to perform the biopsies dissociation. An enzyme mix consisting of enzyme

563 D, enzyme A and buffer L was prepared according to the manufacturer's specifications. Single

564 punch biopsies were incubated in 400 μl of dissociation mix, at 37°C – 5% CO2 overnight.

565 Following incubation, each sample mix was transferred to a Falcon round-bottom tube with cell-

566 strainer cap (40-75um). Using a rubber pestle and the cell-strainer cap as a mortar, biopsies where

567 gently macerated to increase cell recovery yield. 500 μl of cold RMPI was used to rinse caps.

568 Samples were then centrifuged at 1500 rpm 4°C for 10 minutes and the pellet resuspended in 500

569 μl of cold RPMI. Dissociated skin cells were counted using a pre-programmed setting in a

570 Countess™ II FL Automated Cell Counter.

571 **Flow cytometry**

572 Dissociated cells were seeded on round bottom 96-well plates and washed with 200 μl of

573 ThermoFisher's PBS buffer 1x (1500 rpm, 4°C for 5 minutes). Twenty μl of Biolegend Zombie

574 Aqua fixable viability stain (1:500) was added and incubated for 20 minutes in the dark at 4°C.

575 Excess viability stain was washed away with 200 μl of PBS/BSA/EDTA buffer (1500 rpm, 4°C

576 for 5 minutes), and the pellet resuspended and incubated for 10 minutes at 4°C in 4 μl of

577 Biolegend's FcR blocking antibody (1:10). Cells were then incubated for 30 minutes at 4°C with

578 surface staining antibody master mix. After washing free unbound antibody with 200 μl of PBS

579 (1500 rpm, 4°C for 5 minutes), cells were fixed with 100 μl of Biolegend's fixation buffer 1x for

580 20 minutes at 4°C in the dark. Following fixation, cells were permeabilized and washed with 100

581 μl of Biolegend perm-wash solution 1x (1500 rpm, 4°C for 5 minutes) and the pellet resuspended

582 and incubated for 30 minutes at 4°C in intracellular staining antibody master mix. Stained cells

583 were placed in 200 μl of PBS/BSA/EDTA 1x and visualized on a BD Biosciences FACS Aria II

584 using FACS Diva software. Analysis was performed using BD Biosciences FlowJo software.

585 Antibody panels are described in supplemental material (Supplementary Table 5).

586 **In vitro SGE stimulation and Multiplex cytokine screening**

587   Skin dissociated cells were seeded on round bottom 96-well plates (50.000 cells/well) and treated

588   with SGE (10 µg/mL) or PBS for 24 hours. Cells were stimulated with PMA (0.1µg/mL) and

589   Ionomycin (1µg/mL) or left unstimulated for the last 6 hours of the culture. The supernatants were

590   collected and stored at -20°C. Cytokines in the cell culture supernatants were quantified using

591   Human Th Cytokine Panel (12-plex) (Cat. 741027, BioLegend) according to the manufacturer's

592   instructions. All samples in the experiment were measured in duplicate. Briefly, undiluted

593   supernatants were incubated with beads coated with capture antibodies specific for IL-2, 4, 5, 6,

594   9, 10, 13, 17A, 17F, 22, IFN-γ and TNF-α for 2 hours at room temperature on shaker. After

595   incubation, beads were washed and incubated with biotin-labeled detection antibodies for 1 hour,

596   followed by a final incubation with streptavidin-PE for 30 minutes at room temperature on shaker.

597   Beads were washed and re-suspended with washing buffer. Beads were analyzed by flow

598   cytometry using a FACS Canto cytometer. Analysis was performed using the LEGENDplex

599   analysis software v8.0, which distinguishes between the 12 different analytes on basis of bead size

600   and internal dye.

Statistical analyses

602   Flow cytometry and multiplex cytokine screening data were analyzed using the non-parametric-

603   based tests, Wilcoxon signed-rank and Chi-square test. Correlation analysis was performed with

604   the Pearson's correlation coefficient. Bars indicate median and interquartile range, and p-values

605   *p<0.05, **p<0.01, ***p<0.001. Statistical analysis of RNAseq data is described above.

Acknowledgements

607   We would like to thank the study participants in Kampong Speu, Cambodia. We would also like

608   to acknowledge Noemi Kedei and Maria Hernandez for their assistance in histology and staining

609   as well as Jon Fintzi for statistical review of the clinical protocol.

Competing interests

The authors declare no competing interests.

Author contributions

Conceptualization: F.O., J.E.M., T.C., J.G.V. Methodology: D.G., H.V, S.N., S.C., S.L., J.A.B., F.O., J.E.M.. Investigation: D.G., H.V, J.A.B, S.N., S.C., S.L., A.P., J.G.V., F.O., J.E.M. Visualization: D.G., F.O., J.A.B. Funding acquisition: F.O., J.E.M. Study enrollment and clinical procedures: C.L, S.L., R.S, S.S., S.N., J.M, H.K, R.L. Project administration: C.L., T.C., F.O., J.E.M., Supervision: T.C., D.M, F.O., J.E.M., C.L, R.L., H.R, H.K. Writing original draft: D.G., H.V., T.C., F.O., J.E.M., J.A.B. Writing review and editing: T.C., D.M., C.L., F.O., J.A.B., J.E.M.

All authors contributed to the article and approved the submitted version

Data availability

The Illumina raw reads (fastq files) were loaded at the NCBI Sequence Read Archive with accession numbers SRR18215008 to SRR18215047 and deposited in GenBank under bioproject accession code PRJNA812009. All data generated or analyzed during this study are included in this published article (and its supplementary information files). Clinical trial data is

631 available at https://clinicaltrials.gov/ct2/show/NCT04350905. Flow cytometry data can be made

632 available upon reasonable request directly to the authors.

Bibliography

634 1. WHO. A global brief on vector-borne diseases. *www.who.int* (2020).

635 2. Pierson, T. C. & Diamond, M. S. The continued threat of emerging flaviviruses. *Nat. Microbiol.* **5**,

636 796–812 (2020).

637 3. Ryan, S. J., Carlson, C. J., Mordecai, E. A. & Johnson, L. R. Global expansion and redistribution of

638 Aedes-borne virus transmission risk with climate change. *PLoS Negl. Trop. Dis.* **13**, e0007213 (2019).

639 4. Godoy, R. S. M. *et al.* Dengue and Zika virus infection patterns vary among Aedes aegypti field

640 populations from Belo Horizonte, a Brazilian endemic city. *PLoS Negl. Trop. Dis.* **15**, e0009839

641 (2021).

642 5. Sun, P. *et al.* A mosquito salivary protein promotes flavivirus transmission by activation of

643 autophagy. *Nat. Commun.* **11**, 260 (2020).

644 6. Ha, Y.-R. *et al.* Detection of Heparin in the Salivary Gland and Midgut of Aedes togoi. *Korean J.*

645 *Parasitol.* **52**, 183–188 (2014).

646 7. Schneider, B. S. & Higgs, S. The enhancement of arbovirus transmission and disease by mosquito

647 saliva is associated with modulation of the host immune response. *Trans. R. Soc. Trop. Med. Hyg.*

648 **102**, 400–408 (2008).

649 8. Guerrero, D., Cantaert, T. & Missé, D. Aedes Mosquito Salivary Components and Their Effect on the

650 Immune Response to Arboviruses. *Front. Cell. Infect. Microbiol.* **10**, 407 (2020).

651 9. Manning, J. E. & Cantaert, T. Time to Micromanage the Pathogen-Host-Vector Interface:

652 Considerations for Vaccine Development. *Vaccines* **7**, 10 (2019).

653   10. Vogt, M. B. *et al.* Mosquito saliva alone has profound effects on the human immune system. *PLoS*

654   *Negl. Trop. Dis.* **12**, e0006439 (2018).

655   11. Jin, L. *et al.* Salivary factor LTRIN from Aedes aegypti facilitates the transmission of Zika virus by

656   interfering with the lymphotoxin-β receptor. *Nat. Immunol.* **19**, 342–353 (2018).

657   12. Pingen, M. *et al.* Host Inflammatory Response to Mosquito Bites Enhances the Severity of Arbovirus

658   Infection. *Immunity* **44**, 1455–1469 (2016).

659   13. Schneider, B. S., Soong, L., Zeidner, N. S. & Higgs, S. Aedes aegypti salivary gland extracts modulate

660   anti-viral and TH1/TH2 cytokine responses to sindbis virus infection. *Viral Immunol.* **17**, 565–573

661   (2004).

662   14. Hastings, A. K. *et al.* Aedes aegypti NeSt1 Protein Enhances Zika Virus Pathogenesis by Activating

663   Neutrophils. *J. Virol.* **93**, e00395-19, /jvi/93/13/JVI.00395-19.atom (2019).

664   15. Uraki, R. *et al.* Aedes aegypti AgBR1 antibodies modulate early Zika virus infection of mice. *Nat.*

665   *Microbiol.* **4**, 948–955 (2019).

666   16. McCracken, M. K. *et al.* Route of inoculation and mosquito vector exposure modulate dengue virus

667   replication kinetics and immune responses in rhesus macaques. *PLoS Negl. Trop. Dis.* **14**, e0008191

668   (2020).

669   17. Dudley, D. M. *et al.* Infection via mosquito bite alters Zika virus tissue tropism and replication

670   kinetics in rhesus macaques. *Nat. Commun.* **8**, 2096 (2017).

671   18. Trager, W. Acquired Immunity to Ticks. *J. Parasitol.* **25**, 57 (1939).

672   19. Guilbride, D. L., Guilbride, P. D. L. & Gawlinski, P. Malaria's deadly secret: a skin stage. *Trends*

673   *Parasitol.* **28**, 142–150 (2012).

674   20. Conway, M. J. Type I hypersensitivity promotes Aedes aegypti blood feeding. *Sci. Rep.* **11**, 14891

675   (2021).

676   21. Demeure, C. E. *et al.* Anopheles Mosquito Bites Activate Cutaneous Mast Cells Leading to a Local

677   Inflammatory Response and Lymph Node Hyperplasia. *J. Immunol.* **174**, 3932–3940 (2005).

678   22. Conway, M. J. *et al.* Mosquito Saliva Serine Protease Enhances Dissemination of Dengue Virus into

679   the Mammalian Host. *J. Virol.* **88**, 164–175 (2014).

680   23. Turner, C. T., Lim, D. & Granville, D. J. Granzyme B in skin inflammation and disease. *Matrix Biol.* **75–**

681   **76**, 126–140 (2019).

682   24. Buzza, M. S. *et al.* Extracellular Matrix Remodeling by Human Granzyme B via Cleavage of

683   Vitronectin, Fibronectin, and Laminin. *J. Biol. Chem.* **280**, 23549–23558 (2005).

684   25. Champagne, D. E. Antihemostatic Molecules from Saliva of Blood-Feeding Arthropods. *Pathophysiol.*

685   *Haemost. Thromb.* **34**, 221–227 (2005).

686   26. Lefteri, D. A. *et al. Mosquito saliva sialokinin-dependent enhancement of arbovirus infection through*

687   *endothelial barrier leakage*. http://biorxiv.org/lookup/doi/10.1101/2021.02.19.431961 (2021)

688   doi:10.1101/2021.02.19.431961.

689   27. Davies, L. C., Jenkins, S. J., Allen, J. E. & Taylor, P. R. Tissue-resident macrophages. *Nat. Immunol.* **14**,

690   986–995 (2013).

691   28. Mantovani, A., Sica, A. & Locati, M. Macrophage Polarization Comes of Age. *Immunity* **23**, 344–346

692   (2005).

693   29. Mantovani, A., Biswas, S. K., Galdiero, M. R., Sica, A. & Locati, M. Macrophage plasticity and

694   polarization in tissue repair and remodelling: Macrophage plasticity and polarization in tissue repair

695   and remodelling. *J. Pathol.* **229**, 176–185 (2013).

696   30. Bardina, S. V. *et al.* Differential Roles of Chemokines CCL2 and CCL7 in Monocytosis and Leukocyte

697   Migration during West Nile Virus Infection. *J. Immunol.* **195**, 4306–4318 (2015).

698   31. Mills, C. D. Anatomy of a Discovery: M1 and M2 Macrophages. *Front. Immunol.* **6**, (2015).

699   32. Lamana, A. *et al.* CD69 Modulates Sphingosine-1-Phosphate-Induced Migration of Skin Dendritic

700   Cells. *J. Invest. Dermatol.* **131**, 1503–1512 (2011).

701   33. Mackay, L. K. *et al.* Cutting Edge: CD69 Interference with Sphingosine-1-Phosphate Receptor

702   Function Regulates Peripheral T Cell Retention. *J. Immunol.* **194**, 2059–2063 (2015).

703   34. Rajarathnam, K., Schnoor, M., Richardson, R. M. & Rajagopal, S. How do chemokines navigate

704   neutrophils to the target site: Dissecting the structural mechanisms and signaling pathways. *Cell.*

705   *Signal.* **54**, 69–80 (2019).

706   35. Dey, R. *et al.* Gut Microbes Egested during Bites of Infected Sand Flies Augment Severity of

707   Leishmaniasis via Inflammasome-Derived IL-1β. *Cell Host Microbe* **23**, 134-143.e6 (2018).

708   36. Gough, P., Ganesan, S. & Datta, S. K. IL-20 Signaling in Activated Human Neutrophils Inhibits

709   Neutrophil Migration and Function. *J. Immunol.* **198**, 4373–4382 (2017).

710   37. Myles, I. A. *et al.* Signaling via the IL-20 receptor inhibits cutaneous production of IL-1β and IL-17A

711   to promote infection with methicillin-resistant Staphylococcus aureus. *Nat. Immunol.* **14**, 804–811

712   (2013).

713   38. Lefteri, D. A. *et al.* Mosquito saliva enhances virus infection through sialokinin-dependent vascular

714   leakage. *Proc. Natl. Acad. Sci.* **119**, e2114309119 (2022).

715   39. Kirkpatrick, B. D. *et al.* The live attenuated dengue vaccine TV003 elicits complete protection against

716   dengue in a human challenge model. *Sci. Transl. Med.* **8**, (2016).

717   40. Shimizu, K. *et al.* PD-1 Imposes Qualitative Control of Cellular Transcriptomes in Response to T Cell

718   Activation. *Mol. Cell* **77**, 937-950.e6 (2020).

719   41. Wei, F. *et al.* Strength of PD-1 signaling differentially affects T-cell effector functions. *Proc. Natl.*

720   *Acad. Sci.* **110**, E2480–E2489 (2013).

721   42. Duyen, H. T. L. *et al.* Skin dendritic cell and T cell activation associated with dengue shock syndrome.

722   *Sci. Rep.* **7**, 14224 (2017).

723 43. Rivino, L. *et al.* Virus-specific T lymphocytes home to the skin during natural dengue infection. *Sci.*

724   *Transl. Med.* **7**, (2015).

725 44. Mommert, S., Schaper, J. T., Schaper-Gerhardt, K., Gutzmer, R. & Werfel, T. Histamine Increases Th2

726   Cytokine-Induced CCL18 Expression in Human M2 Macrophages. *Int. J. Mol. Sci.* **22**, 11648 (2021).

727 45. Styer, L. M. *et al.* Mosquito Saliva Causes Enhancement of West Nile Virus Infection in Mice. *J. Virol.*

728   **85**, 1517–1527 (2011).

729 46. Chiffoleau, E. C-Type Lectin-Like Receptors As Emerging Orchestrators of Sterile Inflammation

730   Represent Potential Therapeutic Targets. *Front. Immunol.* **9**, 227 (2018).

731 47. Holmskov, U., Thiel, S. & Jensenius, J. C. Collectins and Ficolins: Humoral Lectins of the Innate

732   Immune Defense. *Annu. Rev. Immunol.* **21**, 547–578 (2003).

733 48. Tang, L. *et al.* Liver Sinusoidal Endothelial Cell Lectin, LSECtin, Negatively Regulates Hepatic T-Cell

734   Immune Response. *Gastroenterology* **137**, 1498-1508.e5 (2009).

735 49. Kuo, P. T. *et al.* The Role of CXCR3 and Its Chemokine Ligands in Skin Disease and Cancer. *Front.*

736   *Med.* **5**, 271 (2018).

737 50. Niyonsaba, F., Ogawa, H. & Nagaoka, I. Human beta-defensin-2 functions as a chemotactic agent for

738   tumour necrosis factor-alpha-treated human neutrophils. *Immunology* **111**, 273–281 (2004).

739 51. Niyonsaba, F., Iwabuchi, K., Matsuda, H., Ogawa, H. & Nagaoka, I. Epithelial cell-derived human β-

740   defensin-2 acts as a chemotaxin for mast cells through a pertussis toxin-sensitive and phospholipase

741   C-dependent pathway. *Int. Immunol.* **14**, 421–426 (2002).

742 52. Rizzo, C. *et al.* IgG1 and IgG4 Antibody Responses to the Anopheles gambiae Salivary Protein gSG6 in

743   the Sympatric Ethnic Groups Mossi and Fulani in a Malaria Hyperhendemic Area of Burkina Faso.

744   *PLoS ONE* **9**, e96130 (2014).

745 53. McKimmie, C. S., Pingen, M., Bryden, S. R. & Lefteri, D. A. Host inflammatory response to mosquito

746   bites enhances the severity of arbovirus infection. *ISBT Sci. Ser.* **13**, 76–79 (2018).

747 54. Henrique, M. O. *et al.* Evaluation of inflammatory skin infiltrate following *Aedes aegypti* bites in

748   sensitized and non-sensitized mice reveals saliva-dependent and immune-dependent phenotypes.

749   *Immunology* **158**, 47–59 (2019).

750 55. Qureshi, A. A. *et al.* Immunomodulatory properties of maxadilan, the vasodilator peptide from sand

751   fly salivary gland extracts. *Am. J. Trop. Med. Hyg.* **54**, 665–671 (1996).

752 56. Gillespie, R. D., Dolan, M. C., Piesman, J. & Titus, R. G. Identification of an IL-2 binding protein in the

753   saliva of the Lyme disease vector tick, Ixodes scapularis. *J. Immunol. Baltim. Md 1950* **166**, 4319–

754   4326 (2001).

755 57. Oliveira, F. *et al.* Delayed-Type Hypersensitivity to Sand Fly Saliva in Humans from a Leishmaniasis-

756   Endemic Area of Mali Is TH1-Mediated and Persists to Midlife. *J. Invest. Dermatol.* **133**, 452–459

757   (2013).

758 58. Pasparakis, M., Haase, I. & Nestle, F. O. Mechanisms regulating skin immunity and inflammation.

759   *Nat. Rev. Immunol.* **14**, 289–301 (2014).

760 59. Manning, J. E. *et al.* Safety and immunogenicity of a mosquito saliva peptide-based vaccine: a

761   randomised, placebo-controlled, double-blind, phase 1 trial. *The Lancet* S0140673620310485 (2020)

762   doi:10.1016/S0140-6736(20)31048-5.

763 60. Oliveira, F. *et al.* A sand fly salivary protein vaccine shows efficacy against vector-transmitted

764   cutaneous leishmaniasis in nonhuman primates. *Sci. Transl. Med.* **7**, (2015).

765 61. Sajid, A. *et al.* mRNA vaccination induces tick resistance and prevents transmission of the Lyme

766   disease agent. *Sci. Transl. Med.* **13**, eabj9827 (2021).

767 62. Bryden, S. R. *et al.* Pan-viral protection against arboviruses by activating skin macrophages at the

768   inoculation site. *Sci. Transl. Med.* **12**, eaax2421 (2020).

769 63. Bolger, A. M., Lohse, M. & Usadel, B. Trimmomatic: a flexible trimmer for Illumina sequence data.

770   *Bioinformatics* **30**, 2114–2120 (2014).

771   64. Li, B. & Dewey, C. N. RSEM: accurate transcript quantification from RNA-Seq data with or without a

772   reference genome. *BMC Bioinformatics* **12**, 323 (2011).

773   65. Langmead, B. & Salzberg, S. L. Fast gapped-read alignment with Bowtie 2. *Nat. Methods* **9**, 357–359

774   (2012).

775   66. Dobin, A. & Gingeras, T. R. Mapping RNA-seq Reads with STAR. *Curr. Protoc. Bioinforma.* **51**, (2015).

776   67. Love, M. I., Huber, W. & Anders, S. Moderated estimation of fold change and dispersion for RNA-seq

777   data with DESeq2. *Genome Biol.* **15**, 550 (2014).

778   68. Huber, W., von Heydebreck, A., Sultmann, H., Poustka, A. & Vingron, M. Variance stabilization

779   applied to microarray data calibration and to the quantification of differential expression.

780   *Bioinformatics* **18**, S96–S104 (2002).

781   69. Zhu, A., Ibrahim, J. G. & Love, M. I. Heavy-tailed prior distributions for sequence count data:

782   removing the noise and preserving large differences. *Bioinformatics* **35**, 2084–2092 (2019).

783   70. Benjamini, Y. & Hochberg, Y. Controlling the False Discovery Rate: A Practical and Powerful

784   Approach to Multiple Testing. *J. R. Stat. Soc. Ser. B Methodol.* **57**, 289–300 (1995).

785   71. Blighe, K., Rana, S. & Lewis, M. Enhanced Volcano: publication-ready volcano plots with enhanced

786   colouring and labeling. (2021).

787   72. Walter, W., Sánchez-Cabo, F. & Ricote, M. GOplot: an R package for visually combining expression

788   data with functional analysis: Fig. 1. *Bioinformatics* **31**, 2912–2914 (2015).

789   73. Yu, G., Wang, L.-G., Han, Y. & He, Q.-Y. clusterProfiler: an R Package for Comparing Biological

790   Themes Among Gene Clusters. *OMICS J. Integr. Biol.* **16**, 284–287 (2012).

791   74. Yu, G. & He, Q.-Y. ReactomePA: an R/Bioconductor package for reactome pathway analysis and

792   visualization. *Mol. Biosyst.* **12**, 477–479 (2016).

793   75. Kolde, R. Pretty Heatmaps. R package version.

794   76. Sakai, R., Winand, R., Verbeiren, T., Moere, A. V. & Aerts, J. dendsort: modular leaf ordering

795   methods for dendrogram representations in R. *F1000Research* **3**, 177 (2014).

796   77. R Core Team (2021). *R: A language and environment for statistical computing. R Foundation fo*

797   *Statistical Computing, Vienna, Austria*. (The R Foundation).

798